NANO LETTERS

2007
Vol. 7, No. 12
3598−3602

Observation of Microcavity Modes and Waveguides in InP Nanowires Fabricated by Selective-Area Metalorganic Vapor-Phase Epitaxy

Ying Ding,* Junichi Motohisa, Bin Hua, Shinjiroh Hara, and Takashi Fukui

Research Center for Integrated Quantum Electronics (RCIQE) and Graduate School of Information Science and Technology, Hokkaido University, Sapporo 060-0814, Japan

Received July 9, 2007; Revised Manuscript Received September 23, 2007

ABSTRACT

Hexagonal cylindrical InP nanowires with a wurtzite structure were fabricated by selective-area metalorganic vapor-phase epitaxy (SA-MOVPE). The microcavity modes and waveguides in InP nanowires were investigated by photoluminesence (PL) spectra. Optical mode analysis for InP nanowires with different lengths reveals the axial Fabry–Perot cavity in InP nanowires, which were formed between the two end facets of nanowires. In addition, T-branch subwavelength guiding and optical coupling in InP nanowires were observed.

Nanowires (NWs) have attracted increasing attention for their applications in nanoscale optoelectronic devices (e.g., nanolasers,[1] modulators,[2] detectors,[3] sensors,[4] single photon sources, near-field optics, etc.) as well as for realizing miniaturized photonic integrated circuits (PICs). It is important to study the optical cavity and waveguide properties of nanowires for fabricating aforementioned devices and PICs. Admirable results and recent reports on NW lasers are mainly concentrated on the materials of GaN,[5,6] ZnO,[7,8] CdS,[1,9] poly(9,9-dioctylfluorene) (POF),[10] and so forth. These materials all have large band gaps and short wavelength emission from the ultraviolet to cyan region. On the other hand, NW waveguides and optical routing also were realized at the short wavelength band with materials of CdS, GaN, ZnO, and so forth.[2,11,12] Unlike the wide band gap material NWs mentioned above, InP NW emission and waveguides with near-infrared wavelengths are more suitable for the applications of short-distance optical fiber communications, free-space optics, and chip-to-chip or on-chip optical interconnections. Especially for chip level optical interconnections, which have the potential to break through the interconnect bottleneck in high-performance computer systems, InP and InP-based NWs may be the optimal candidate materials for this application. Compared with GaAs NWs with the overlapped wavelength band, InP NWs have more powerful emission and finer waveguiding effects because of the higher density of surface states for GaAs NWs causing considerable nonradiative recombination, which was confirmed by PL measurements of InP and GaAs NWs with the same size in our study. However, it is challenging to obtain the waveguides and the microresonator for NWs at the near-infrared region because a somewhat large fraction of the guided field outside of the NWs as evanescent waves increases the propagation loss and the poor reflectivity of end facets, which, due to the NWs' small size compared with the wavelength, results in a significant mirror losses. In this letter, we fabricated InP nanowires with a wurtzite structure by using SA-MOVPE. Fabry−Perot cavity modes in InP NWs were investigated and verified. The subwavelength guiding and optical coupling in InP nanowires were observed.

The NWs fabricated by the SA-MOVPE method have recently drawn much interest due to the advantage of catalyst-free, high-uniformity, and superior growth controllability.[13−15] Furthermore, a Fabry−Perot (F−P) cavity in a single NW can be formed easily and spontaneously by using the SA-MOVPE method. The fabrication procedure for InP NWs using SA-MOVPE was reported previously.[16,17] In short, the procedure started with the deposition of a 25 nm SiO_2 layer on the InP (111)A substrate. Then, periodic hexagonal opening patterns were formed on the SiO_2 layer by electron beam (EB) lithography and wet etching. Finally, the substrates with the SiO_2 mask were loaded into a horizontal low-pressure MOVPE reactor for selective-area growth, the working pressure of which was 0.1 atm. The growth temperature was 640 °C, and the growth time was 20 min. Trimethylindium (TMI) and tertiarybutylphosphine (TBP) were used for precursors, and the partial pressures of TMI and TBP were 4.4×10^{-6} and 5.7×10^{-5} atm, respectively.

* To whom correspondence should be addressed. Email: ding@rciqe.hokudai.ac.jp.

10.1021/nl071651x CCC: $37.00
Published on Web 11/09/2007

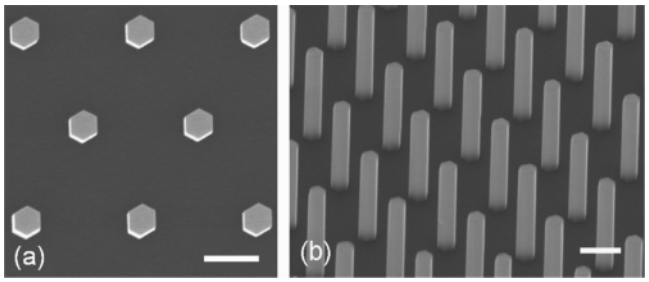

Figure 1. SEM images of free-standing InP NW arrays on an InP (111)A substrate. (a) Top view; (b) tilted view. Scale bar, 500 nm.

Figure 1 shows the scanning electron microscope (SEM) images of a typical as-grown InP NW array on an InP (111)A substrate. The hexagonal cylindrical InP NWs are uniform in length, diameter, shape, and position, with the six {110} vertical facets normal to the top (111)A plane. The diameter of the NW was designed to range between 200 and 250 nm in order to increase the optical confinement and end facets' reflectivity. The actual diameter was slightly larger than it because of the radial growth, more or less. The length of the NWs is from 1 to 6 μm depending on the different selective mask designs.

Before μPL measurements, the free-standing InP NWs were mechanically cut down and dispersed on the Si substrate with metal markers. These metal markers enabled us to locate individual wires and to perform optical measurements and SEM observations on the same nanowires. It should be noted that the optical losses in the Si substrate are negligible here because of the large difference of refractive index between the InP NW and air as well as the relatively large NW diameters resulting in a piddling leakage mode in the substrate, which was verified by the comparison of different substrates of Si and SiO_2 on Si for PL measurements in our investigation. The μPL measurements were carried out from 4 K to room temperature (RT). A He−Ne laser with a wavelength of 632.8 nm was used for excitation. The excitation beam was focused onto a ~2 μm diameter spot with a ×50 microscope objective on the samples placed in a coldfinger cryostat. The excitation power intensity was adjusted using different combinations of neutral density (ND) filters, and the maximum power density on samples was around 1000 W/cm^2. The PL collected through the same microscope objective was detected by a liquid-N_2-cooled charge-coupled device (CCD) for spectral analysis or dispersed into a CCD camera for imaging. A two-dimensional motor was used for moving the sample with a fine moving step of 100 nm.

Room-temperature PL spectra measured from a single InP NW on a Si substrate are shown in Figure 2, with Figure 2a for the NW with a tapered end and Figure 2b for the NW with flat ends. We think that the tapered end in a few NWs in our experiment was formed during the initial stages of the selective growth due to the possible incomplete opening on the SiO_2 layer. In Figure 2a, the NW exhibits a PL peak at 1.435 eV, corresponding to band edge emission, which is 91 meV higher than that of a bulk zinc blende InP (1.344 eV at RT). This value reveals that the crystal structure of

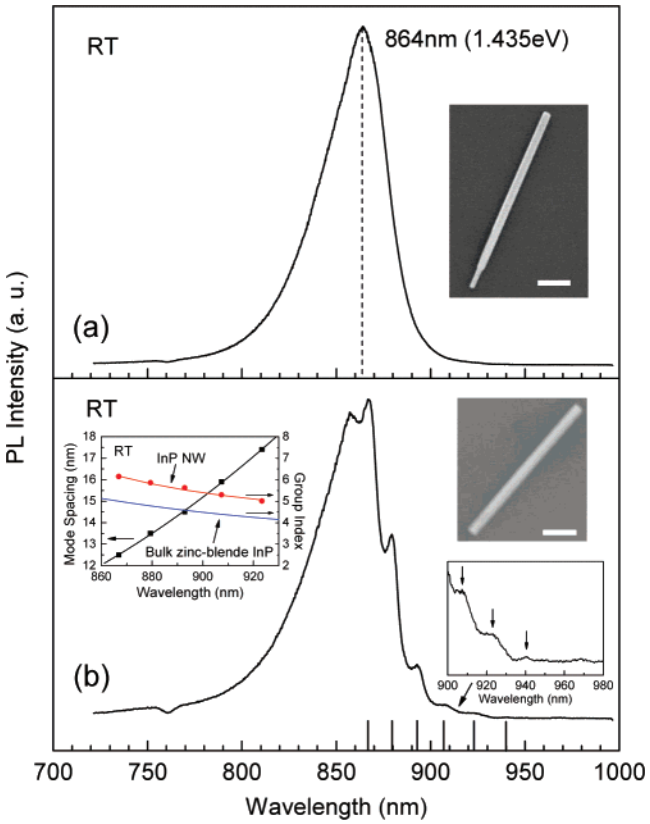

Figure 2. Room-temperature PL spectra of a single InP NW on a Si substrate. (a) NW with a tapered end. (b) NW with flat ends; sticks below spectrum denote the cavity modes. Left inset in (b) is the relation between the measured modes spacing, the group index of the InP NW, the group index of bulk zinc blende InP, and the wavelength. The spectrum inset in (b) is the local magnified spectrum. Image inset: the SEM images of the NW for each spectrum. Scale bar, 1 μm.

the InP NW is wurtzite, which is almost consistent with the theoretically calculated value.[18] TEM observation also revealed the wurtzite structure of the InP NW in our previous study.[17] In Figure 2b, the NW exhibits a similar PL spectrum, except periodic peaks (optical modes) appeared at the low-energy side of the spectrum, which indicates the distinctly resonant effect.

Comparing the two PL spectra in Figure 2, we suppose the optical modes that appeared in Figure 2b formed by the optical reflection from the end facets of an InP NW, that is, an axial Fabry−Perot (F−P) cavity modes was formed in the InP NW with flat ends. Accordingly, there no periodic peaks appeared in the PL spectrum of the NW with the tapered end, whereas almost all of the NWs with flat ends exhibited cavity-mode-modulated PL spectra, more or less.

The spacing of modes in the F−P cavity is given by

$$d\lambda_0 = \frac{{\lambda_0}^2}{2nL\left[1 - \left(\frac{\lambda_0}{n}\right)\left(\frac{dn}{d\lambda_0}\right)\right]} \quad (1)$$

where L is the NW length and n is the refractive index. The mode spacing versus wavelength obtained from the PL

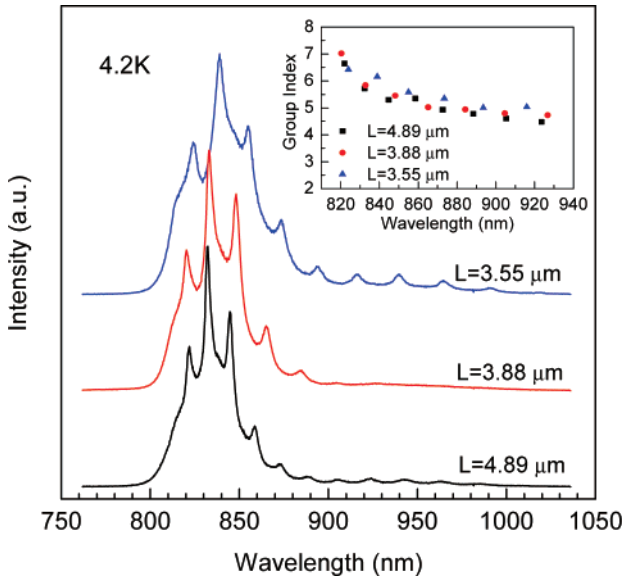

Figure 3. PL spectra of InP NWs with different lengths at 4.2 K. Inset: wavelength dependence of group indices of InP NWs.

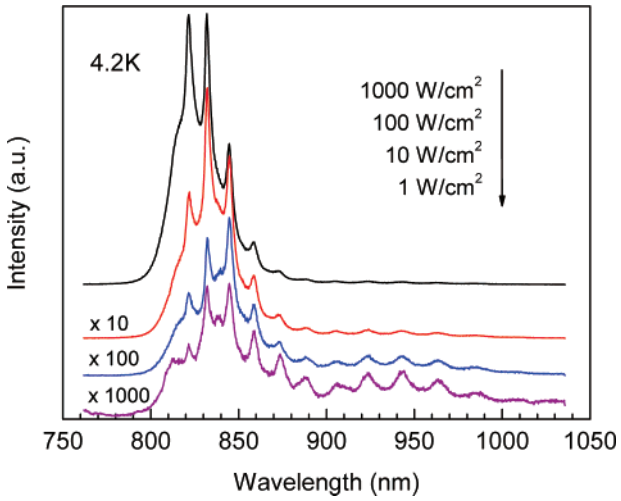

Figure 4. Excitation power density dependence of PL spectra recorded from a single InP NW at 4.2 K.

spectrum in Figure 2b is plotted in the left inset of it. The relation between the group index ($n_g = n - \lambda_0 \cdot (dn/d\lambda_0)$) of the InP NW and the wavelength based on eq 1 is also shown in the same inset. For comparison, the wavelength dependence of the group index of the bulk zinc blende InP is simultaneously given, which was calculated from the Sellmeier formula.[19] As seen, the group index of the InP NW is somewhat higher than that of bulk zinc blende InP. The possible reason for this difference is attributed to the different crystal structure (wurtzite vs zinc blende) and anisotropy of the refractive index. The curvilinear trend of the group index of the InP NW is consistent with that of bulk zinc blende InP and indicates that the supposition of F−P cavity modes in the wurtzite InP NW is reasonable.

PL spectra measured from InP NWs with different lengths at 4.2 K are shown in Figure 3. The diameters of the measured InP NWs all are around 300 nm. The excitation power density is 100 W/cm^2. As expected, the mode spacing increases with the decreasing wire length for different InP NWs, and it is proportional to the inverse wire length. This further verifies that the optical modes are axial F−P cavity modes. According to the mode spacing versus wavelength, we calculate the relation between group indices of InP NWs and the wavelength for different wire lengths based on the eq 1 (Figure 3 inset). From the inset of Figure 3, we obtain the approximate values of group indices for wurtzite InP NWs, which change from 4.5 to 7 with the wavelength ranging from 820 to 930 nm at 4.2 K. The refractive index of the wurtzite InP NW can be determined by a nonlinear curve fit through the formula $n_g = n - \lambda_0 \cdot (dn/d\lambda_0)$ and the Sellmeier equation $n^2 = A + B \cdot \lambda_0^2/(\lambda_0^2 - C)$, which will be useful for the design of InP NW-based nanoscale optoelectronic circuits, such as a hybrid NW photonic crystal.[20]

However, for further short NWs with the length of 1 μm−2 μm, the mode spacing (not shown here) continues to increase but no longer follows the inverse wire length dependence very well, which agrees with the reported result of short ZnO nanoribbons.[21] It can be understood that the wire length is too short to be regarded as a strict F−P cavity, and eq 1 is not applicable.

By multiple-peaks Lorentzian fitting for PL spectra, we obtain the width of each mode and then calculate the mode quality factor (Q factor). The long NW exhibits a relatively high cavity mode Q factor compared with that from the short NW. Since the Q factor is directly related to the cavity losses, relatively low mirror losses ($\alpha = 1/L \cdot \ln(1/R)$) for a long cavity lead to a relatively high Q factor. Hence, the longer wires are expected for an enhanced Q factor.

In Figure 4, we give the excitation power density dependence of PL spectra recorded from a single InP NW with the length of 4.89 μm and a diameter of 300 nm at 4.2 K. The peak position of the cavity modes does not change under the different excitation power density, which indicates that the stable cavity mode characteristics, that is, the refractive index, do not change with the increasing optical pumping rate. The main modes shift to 821 and 832 nm (somewhat longer than the PL peak position of ~815 nm from InP NW without resonance), and long-wavelength modes almost disappeared with the increasing pumping intensity. This may be caused by the increase of gain for the modes near the gain peak and the increase of the cavity loss as well as the low gain for long-wavelength modes.

With the increase of the excitation power density from 10 to 100 to 1000 W/cm^2 (the maximum available value in this measurement), the corresponding mode Q factors are calculated to be 110, 137, and 173 at 832.3 nm by Lorentzian fitting for PL spectrum, as shown in Figure 4. Furthermore, the corresponding mode losses are estimated to be 3916, 3144, and 2490 cm^{-1} according to the relation between the Q factor and the mode loss.[22,23] The cavity mode becomes narrow but does not collapse to a sharp lasing mode with the increase of pumping intensity, indicating the cavity mode loss is too large to be overcome by the mode gain. We believe that further optimization of the InP NW with a longer length or with a distributed Bragg reflector (DBR)[24,25] has the potential to achieve lasing.

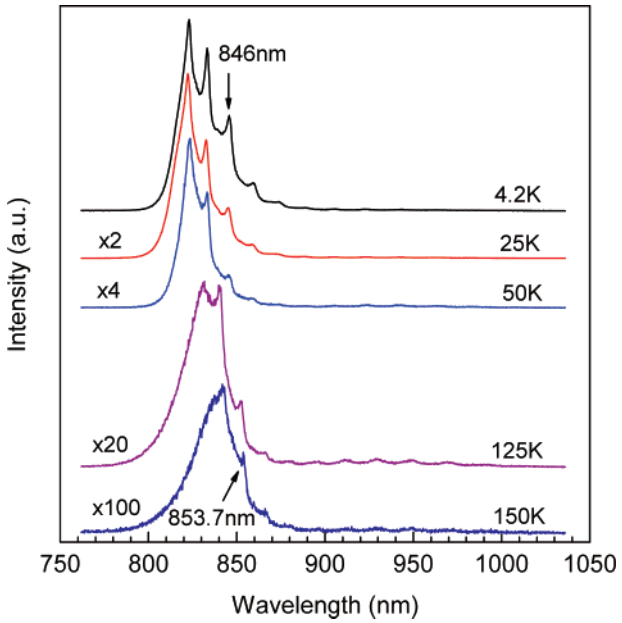

Figure 5. Temperature dependence of PL spectra recorded from a single InP NW.

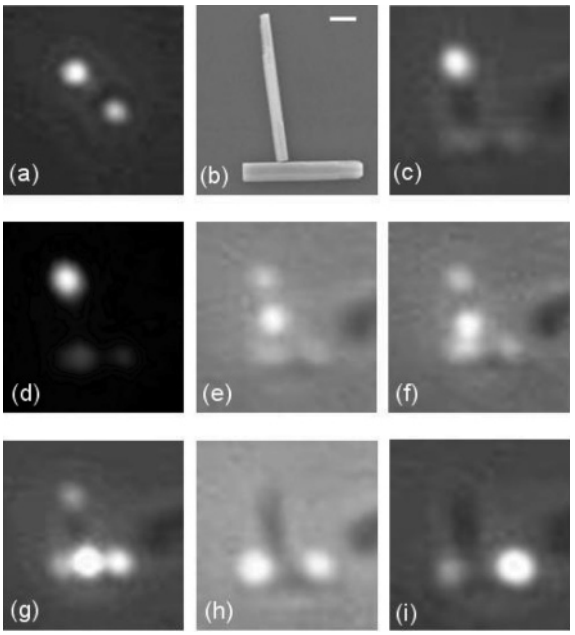

Figure 6. Luminescence images of InP NWs under an excitation power density of 1000 W/cm^2. (a) A single InP NW under optical excitation. (b) SEM image of a reversed T-branch consisting of two InP NWs. Scale bar, 1 μm. (c−i) Luminescence image of T-branch waveguides recorded during the moving process of the excitation laser spot from the upper wire to the nether wire.

The shifts of the modes' peak position with the change of temperatures from a single InP NW are presented in Figure 5. From 4 to 150 K, the red shift of the cavity mode is around 7.7 nm, which is smaller than the red shift of the band edge transition peak of about 14 nm for the wurtzite InP NW. This is due to the small change of refractive index with the change of temperature. The deformation of the mode peak at 150 K is caused by the effect of a larger shift of the band edge transition peak.

In addition, we investigate the subwavelength guiding in a single InP NW and optical coupling between InP NWs. Luminescence from the InP NW was observed and recorded by CCD camera with a laser filter. From Figure 6a, we can see the luminescence spots at the two ends of the InP NW with the excitation laser focused on the center of the NW. More than 80% of NWs with diameters of 200−400 nm show distinct ends luminescence in the measurements. The localization of bright spontaneous emission at the two ends of the wire suggests the strong waveguiding effect and that the cavity modes are axial F−P modes. Figure 6b shows a reversed T-branch consisting of two InP NWs with a perpendicular position. The T-branch was formed randomly during the dispersion of InP NWs on a Si substrate. The two wires have diameters around 500 and 750 nm, respectively. We focus the excitation laser spot on the top end of the upper wire; the luminescence can be observed at the two ends of the upper wire and at the nether wire, as shown in Figure 6c (with LED background light) and d (without LED background light). This means that the light propagated from the top end of the upper wire to the bottom end of the upper wire then coupled to the nether wire and then emitted from the two ends of the nether wire. With the move of the excitation laser spot from the middle of the upper wire (Figure 6e) to the underside of the upper wire (Figure 6f) to the crossing of the two wires (Figure 6g), the luminescence spots from the ends of both wires can be seen. In these instances, the luminescence from the excitation spot also can be observed. When we move the laser spot to the left end of the nether wire (Figure 6h) or right end of the nether wire (Figure 6i), only two luminescence spots can be observed at the two ends of the nether wire, indicating that the light propagated along the nether wire axis and emitted at the two ends of nether wire. There is no observable light coupled from the nether wire to the upper wire. The reason for this can be explained by the fact that the upper NW does not cause an effective increase of the refractive index at the upside of the crossing part. Therefore, the wavefront changes little during its propagation in the nether wire. In fact, the T-branch waveguides can be regarded as special Y-branch waveguides with two 90° branch angels (along the vertical direction) or asymmetrical Y-branch waveguides with one 0° branch angle and one 90° branch angel (along the horizontal direction). In this way, the light propagation and power division in the T-branch waveguides will be understood easily.

All of the results shown in Figure 6 illustrate that the InP NWs can sustain light with a vacuum wavelength larger than the wire diameters, and the T-branch waveguides enable light to be guided through sharp 90° corners. Further, the modes with near band edge energies guided in InP NWs can be regarded as "active waveguides",[2] which has the promise to be used for optical switches or modulators. Although further investigations are required to ascertain the waveguides loss, this is the first time the experimental demonstration of waveguides and optical coupling in InP NWs at the near-infrared band has been given, which has the potential to open the way toward the realization of micron-scale PICs at the near-infrared region.

In conclusion, we fabricated hexagonal cylindrical InP NWs with wurtzite structure by SA-MOVPE. By analyzing the optical modes from several different InP NWs, it was concluded that the axial F−P cavity modes are formed between the two facets of NWs. We discussed the characteristics of microcavity modes in InP NWs. The cavity mode Q factor and mode losses were estimated. Increasing the NWs' length or adopting DBR will improve the Q factor and has the potential to achieve lasing. In addition, T-branch waveguides in InP NWs were formed. We observed the optical propagation and coupling in these T-branch waveguides, which is useful for the applications of PICs.

Acknowledgment. The authors would like to thank Professor K. Hiruma, Dr. L. Yang, Mr. K. Tomioka, Mr. J. Noborisaka, Mr. Y. Kobayashi, and Mr. M. Fukui for valuable discussions and experimental support.

References

(1) Duan, X.; Huang, Y.; Agarwal, R.; Lieber, C. M. *Nature* **2003**, *421*, 241.
(2) Barrelet, C. J.; Greytak, A. B.; Lieber, C. M. *Nano Lett.* **2004**, *4*, 1981.
(3) Soci, C.; Zhang, A.; Xiang, B.; Dayeh, S. A.; Aplin, D. P. R.; Park, J.; Bao, X. Y.; Lo, Y. H.; Wang, D. *Nano Lett.* **2007**, *7*, 1003.
(4) Wang, X.; Zhou, J.; Song, J.; Liu, J.; Xu, N.; Wang, Z. L. *Nano Lett.* **2006**, *6*, 2768.
(5) Gradecak, S.; Qian, F.; Li, Y.; Park, H. G.; Lieber, C. M. *Appl. Phys. Lett.* **2005**, *87*, 173111.
(6) Pauzauskie, P. J.; Sirbuly, D. J.; Yang, P. *Phys. Rev. Lett.* **2006**, *96*, 143903.
(7) Huang, M. H.; Mao, S.; Feick, H.; Yan, H.; Wu, Y.; Kind, H.; Weber, E.; Russo, R.; Yang, P. *Science* **2001**, *292* 1897.
(8) Van Vugt, L. K.; Ruhle, S.; Vanmaekelbergh, D. *Nano Lett.* **2006**, *6*, 2707.
(9) Agarwal, R.; Barrelet, C. J.; Lieber, C. M. *Nano Lett.* **2005**, *5*, 917.
(10) O'Carroll, D.; Lieberwirth, I.; Redmond, G. *Nat. Nanotechnol.* **2007**, *2*, 180.
(11) Greytak, A. B.; Barrelet, C. J.; Li, Y.; Lieber, C. M. *Appl. Phys. Lett.* **2005**, *87*, 151103.
(12) Sirbuly, D. J.; Law, M.; Pauzauskie, P.; Yan, H. Q.; Maslov, A. V.; Knutsen, K.; Ning, C. Z.; Saykally, R. J.; Yang, P. D. *Proc. Natl. Acad. Sci. U.S.A.* **2005**, *102*, 7800.
(13) Noborisaka, J.; Motohisa, J.; Hara, S.; Fukui, T. *Appl. Phys. Lett.* **2005**, *87*, 093109.
(14) Mohan, P.; Motohisa, J.; Fukui, T. *Appl. Phys. Lett.* **2006**, *88*, 013110.
(15) Mohan, P.; Motohisa, J.; Fukui, T. *Appl. Phys. Lett.* **2006**, *88*, 133105.
(16) Inari, M.; Takeda, J.; Motohisa, J.; Fukui, T. *Physica E* **2004**, *21*, 620.
(17) Mohan, P.; Motohisa, J.; Fukui, T. *Nanotechnology* **2005**, *16*, 2903.
(18) Murayama, M.; Nakayama, T. *Phys. Rev. B* **1994**, *49*, 4710.
(19) Martin, P.; Skouri, E. M.; Chusseau, L.; Alibert, C. *Appl. Phys. Lett.* **1995**, *67*, 881.
(20) Barrelet, C. J.; Bao, J.; Loncar, M.; Park, H. G.; Capasso, F.; Lieber, C. M. *Nano Lett.* **2006**, *6*, 11.
(21) Yan, H.; Johnson, J.; Law, M.; He, R.; Knutsen, K.; McKinney, J. R.; Pham, J.; Saykally, R.; Yang, P. *Adv. Mater.* **2003**, *15*, 1907.
(22) Huang, Y. Z.; Chen, Q.; Guo, W. H.; Lu, Q. Y.; Yu, L. J. *IEEE J. Sel. Top. Quantum Electron.* **2006**, *12*, 59.
(23) Wang, M. Q.; Huang, Y. Z.; Chen, Q.; Cai, Z. P. *IEEE J. Quantum Electron.* **2006**, *42*, 146.
(24) Chen, L.; Towe, E. *Appl. Phys. Lett.* **2006**, *89*, 053125.
(25) Gerard, J. M.; Sermage, B.; Gayral, B.; Legrand, B.; Costard, E.; Thierry-Mieg, V. *Phys. Rev. Lett.* **1998**, *81*, 1110.

NL071651X